CMS Physics Analysis Summary

Contact: cms-pag-conveners-susy@cern.ch 2012/09/12

SUSY Search in Photon(s)+jets+$E_{\mathrm{T}}^{\mathrm{miss}}$ final state with the Jet-Gamma Balance method

The CMS Collaboration

Abstract

This paper presents a search for supersymmetry in final states with at least one photon, jets and missing transverse energy, using 2011 data samples of pp collisions at $\sqrt{s} = 7$ TeV, collected by the *CMS* detector at the Large Hadron Collider. The data samples correspond to 4.7 fb^{-1}. A new approach is used to establish the presence of the signal over background and estimate the background from the data, the Jet-Gamma Balance method. We observe no significant deviations from the SM expectation and derive upper limits on the signal cross section at the 95% confidence level for a range of squark, gluino and neutralino mass points in the Gauge Mediated Supersymmetry Breaking (GMSB) scenario.

1 Introduction

The analysis documented in this paper searches for supersymmetry (SUSY) in the γ + jets and missing transverse energy ($E_{\mathrm{T}}^{\mathrm{miss}}$) final state produced by events in 7 TeV pp interactions, collected by the *CMS* detector at the Large Hadron Collider. This is an experimentally accessible channel since photons can be identified with relatively high efficiency and purity at hadron collider experiments. An additional factor is that in the case of missing transverse energy, something that is expected by SUSY scenarios [1–3], the Standard Model backgrounds are largely suppressed.

According to the General Gauge-Mediation (GGM) SUSY scenario investigated in this paper, the gravitino is the lowest mass SUSY particle (LSP) and the lightest neutralino is the next-to-lowest mass SUSY (NLSP) particle. In this paper we are studing bino and wino-like neutralinos.

A bino-like neutralino decays predominantly into a gravitino and a photon with a branching fraction $\backsim cos^2\theta_{\mathrm{w}}$, while the decay to a gravitino and a Z boson is sub-dominant ($\backsim sin^2\theta_{\mathrm{w}}$). In the case of a wino-like neutralino, the splitting between the charged and the neutral wino is in general small. Thus the neutral and charged winos become co-NLSPs, meaning that the charged winos decay directly into the gravitino and a W^+/W^- as well, while the neutral decay dominantly to a gravitino and a Z boson ($\backsim cos^2\theta_{\mathrm{w}}$) and sub-dominantly to a gravitino and a photon ($\backsim sin^2\theta_{\mathrm{w}}$).

We only consider cases in which at least one of the neutralinos decays promptly to a gravitino and a photon. Since the gravitino escapes detection, it leads to missing transverse energy in the event. Assuming R-parity conservation, SUSY particles are pair produced. Those particles are dominantly strongly interacting with decay chains including one or several quarks/gluons. Therefore, events with a pure bino-like neutralino are expected to contain two photons and two gravitinos plus additional Standard Model particles in the final states. The created Standard Model particles are either a photon or a Z or a Higgs boson if the mass difference between the NLSP and the LSP allows it kinematically. A second signature, with just one photon, is possible if one of the NLSPs decays into a Z boson instead of a photon. Lastly in the case of a wino-like neutralino, the di-photon final state is quite suppressed but single-photon final states may be significant.

A new approach is used to establish the presence of the signal over background and estimate the background from the data, the Jet-Gamma Balance (JGB) method, which is explained in more details in Section 5. The Jet-Gamma Balance variable, can be thought of as $E_{\mathrm{T}}^{\mathrm{miss}}$ with sign information. Our topology of interest is at least one isolated photon, jets and $E_{\mathrm{T}}^{\mathrm{miss}}$. This signature of SUSY signal events can be mimicked by various backgrounds. Processes with rare reconstruction effects but with huge cross sections, such as photons plus jets, can give apparent $E_{\mathrm{T}}^{\mathrm{miss}}$ due to detector resolution (poorly measured hadronic activity in the event). Another background comes from processes with real $E_{\mathrm{T}}^{\mathrm{miss}}$ such as $t\bar{t}$ and electroweak events with a leptonic $W \rightarrow e\nu$ decay, where one electron can be misidentified as a photon and neutrinos lead to $E_{\mathrm{T}}^{\mathrm{miss}}$, since they escape detection. Drell Yan events can also contribute to this kind of background. Additional backgrounds can occur due to initial and final state radiation of photons. The dominant contribution comes from $t\bar{t}$ or W/Z events with one or more neutrinos in the final state. Events where the W/Z bosons decay hadronically usually do not pass the JGB requirement.

2 Standard Model Backgrounds and Benchmark Signals

The backgrounds contributing to the γ + jets + $E_{\mathrm{T}}^{\mathrm{miss}}$ final state are listed below:

- γ **+ jets/multi jets**: Dominant Standard Model background that can give apparent $E_{\mathrm{T}}^{\mathrm{miss}}$ due to detector resolution and reconstruction effects.
- **W + jets**: This background along with $t\bar{t}$ + jets and Drell-Yan is sub-dominant and includes processes with real $E_{\mathrm{T}}^{\mathrm{miss}}$. The decays of the charged $W^{+/-}$ bosons that may contribute to our standard model background are: $W \to e\nu$ where the electron may fake the photon and $W \to \tau\nu$ when $\tau \to e\nu\nu$, or $\tau \to h \geq 1\pi^0\nu$.
- **t$\bar{\mathbf{t}}$ + jets**: The top quark decays through the weak interaction producing a W-boson and a down-type quark (principally bottom but also down and strange quark)[4]. The produced Ws may induce a background to our signal due to the electron (to photon) mistagging and the escaping neutrino.
- γ **+ W/Z + jets**: The presence of W/Zs may also induce a background, where the missing transverse energy is present due to neutrinos.
- **Drell Yan + jets**: In proton proton collisions, $q\bar{q}$ interaction may produce Z^0 or $\gamma^\star$ which subsequently decay to a lepton antilepton pair. This process, known as Drell-Yan process is a potential background.

Three different signal scenarios have been used as benchmarks, two bino-like and one wino-like neutralino (Tab. 1). For the first bino-like scenario, the neutralino mass was fixed to 375 GeV and the squark as well as the gluino masses were varying from 400 to 2000 GeV, while for the second the mass of the squark was fixed to 2500 GeV and the neutralino and gluino masses were varying. The wino-like neutralino scenario has fixed neutralino mass (375 GeV) and varying squark and gluino masses.

Table 1: Summary of studied GGM benchmark scenarios

	$\mathrm{m}_{neutralino}$[GeV]	m_{squark}[GeV]	m_{gluino}[GeV]
bino-like	375	400-2000	400-2000
bino-like	150-1050	2500	160-2000
wino-like	375	400-2000	400-2000

Since mismeasured $E_{\mathrm{T}}^{\mathrm{miss}}$ can mimic signal events, our ability to establish the presence of a signal over background relies on accurate prediction of the missing energy tail of this background. The rate of the mismeasured background is difficult to estimate using Monte Carlo simulation alone. In this paper we present a data-driven approach, the Jet-Gamma Balance (JGB) method, inspired by the SUSY leptonic searches in Z+jets+$E_{\mathrm{T}}^{\mathrm{miss}}$ final state [5, 6].

This paper is organized as follows: Description of the objects and event selection followed by a description of the Jet-Gamma Balance method. Afterwards there is a presentation of the full background estimation method and its validation on Monte Carlo simulation and finally a discussion of the results of the search and the related systematic uncertainties.

3 The CMS detector

The Compact Muon Solenoid (CMS) detector operates at the Large Hadron Collider (LHC) at CERN, with overall dimensions 21.6 m in length, 14.6 m in diameter and total weight of 12500 t. The central feature of the CMS apparatus is a superconducting solenoid (6 m internal diameter), which provides an axial magnetic field of 3.8 T along the beam direction. Charged particle trajectories are measured by the inner tracking system, which is composed of a pixel detector and a silicon strip tracker, covering $0 < \phi < 2\pi$ in azimuth and $|\eta| < 2.5$ (pseudorapidity $\eta = -ln[tan\theta/2]$, θ is the polar angle of the trajectory of the particle with respect to the beam direction). The tracking system is surrounded by a crystal electromagnetic calorimeter (ECAL) and a brass/scintillator hadron calorimeter (HCAL). The ECAL consists of 61200 lead tungstate ($PbWO_4$) crystals mounted in the central barrel part, closed by 7324 crystals in each of the two endcaps. It provides coverage in pseudorapidity $|\eta| < 1.479$ in the barrel and $1.479 < |\eta| < 3.0$ in the two endcap regions. A preshower detector is placed in front of the endcap crystals in order to identify neutral pions within a fiducial region $1.653 < |\eta| < 2.6$. It also helps to distinguish electrons from minimum bias ionizing particles and allows the position determination of electrons and photons with its high granularity. The hadron calorimeter (HCAL) barrel extends radially from the outside of the ECAL to the inner radius of the magnet coil and it covers the pseudorapidity range $|\eta| < 1.3$, while the HCAL endcaps cover the range $1.3 < |\eta| < 3$. Muons are measured in gas detectors embedded in the steel return yoke outside the solenoid. The CMS detector is nearly hermetic, allowing for reliable energy balance measurements in the plane transverse to the beam directions. A two-level trigger system selects the most interesting pp colision events. A more detailed description of the CMS detector can be found in Ref. [7].

4 Data Sample and Event Selection

The data used in this analysis are accumulated using a set of triggers which require at least one photon with transverse momentum $p_{\mathrm{T}} > 70\,\mathrm{GeV}$ and a minimum of hadronic transverse energy (H_{T}) requirement that increased over the course of the run to a final value of 400 GeV. H_{T} is defined as the scalar p_{T} sum of all the jets detected in the HCAL with $p_{\mathrm{T}} > 40\,\mathrm{GeV}$, $|\eta| < 3$ and satisfying quality requirements. The offline cuts are more restrictive than the trigger requirements to ensure good understanding of the efficiency. The corresponding luminosity is 4.7 fb^{-1}.

In the following paragraphs we briefly describe the physics object selection.

The photon candidates are reconstructed from clusters of energy in the CMS electromagnetic crystal calorimeter (ECAL). The ECAL was designed to have both excellent energy resolution and high granularity, making it a powerful instrument to measure photons with high precision at the LHC. Photon objects are created based on depositions of energy within the ECAL. Because of the material in front of the calorimeter, photon conversions and bremsstrahlung from electrons and positrons is likely. The strong magnetic field often leads the energy flow associated with primary electrons or converted primary photons to spread in ϕ. To collect the photon energy in the ECAL, local deposits are summed into superclusters that are extended in ϕ. A supercluster passing a list of identification and quality criteria (e.g. shower shape) is promoted to a photon as discribed in [8]. In addition, the absence of a pixel tracker hits matching to the supercluster is required to descriminate photons from electrons. To increase the purity of the photon sample, isolation requirements are applied using combined information from ECAL, HCAL and the tracker. In total, not more than 6 GeV pile-up subtracted [9] energy deposit is allowed within a cone of $\Delta R = \sqrt{\Delta\phi^2 + \Delta\eta^2} = 0.3$.

The definition of an electron is similar to a photon except for the requirement of hits on the pixel tracker matching to the supercluster. Electrons are used to estimate the backgrounds from processes with an electron misidentified as photon and real $E_{\mathrm{T}}^{\mathrm{miss}}$ (e.g. $W \to e\nu$) similarly to [10] and references within.

Jets are clustered with the anti-k$_T$ clustering algorithm [11] with a size parameter $R = 0.5$ and reconstructed with the Particle-Flow reconstruction algorithm [12]. Energy scale corrections are applied in the jet to take into account the non-linear jet energy response [13]. For the H_{T} offline selection, calorimeter jets (jets reconstructed using only the energy deposits in the calorimeter towers) are used in order to follow the online selection. Within the Particle-Flow framework the $E_{\mathrm{T}}^{\mathrm{miss}}$ is the p_{T} of the negative vector sum of all reconstructed particles [12].

We select events with at least one photon and at least three jets with acceptance as listed below:

- at least one photon with $p_{\mathrm{T}} > 80$ GeV, $|\eta| < 1.4442$
- at least three jets with $p_{\mathrm{T}} > 100$ GeV, $|\eta| < 2.6$ with a distance $\Delta R > 0.4$ from the photon candidate
- $H_{\mathrm{T}} > 460\,\mathrm{GeV}$.

5 Background Estimation

Prior to applying the analysis procedure to the data, a Monte Carlo closure test was performed for the background only and the signal+background hypothesis. MC simulated samples produced with the MADGRAPH generator [14] are used to study the performance and the systematic uncertainties on the background estimation. The simulated samples are re-weighted to reflect the data luminosity and the beam conditions due to pile-up of minimum bias interactions.

The JGB observable is defined as:

$$JGB = |\sum \overrightarrow{p_{\mathrm{T}}, jets}| - |\overrightarrow{p_{\mathrm{T}}, \gamma}| = |\overrightarrow{E_{\mathrm{T}}^{\mathrm{miss}}} + \overrightarrow{p_{\mathrm{T}}, \gamma}| - |\overrightarrow{p_{\mathrm{T}}, \gamma}| \quad (1)$$

Figure 1 shows the JGB distribution for five different signals and the most important SM backgrounds. A high positive value of JGB favors events with a photon produced at the end of a decay chain (e.g. SUSY cascade decay). Photons produced closer to the primary interaction are kinematically balanced and tend to produce JGB close to zero. SM backgrounds with only mismeasured $E_{\mathrm{T}}^{\mathrm{miss}}$ are evenly poppulating JGB > 0 and JGB < 0 regions. Thus the region with JGB < 0 can be used as a control sample to model the background event yield expected in JGB > 0. The precision of this approach improves for high jet multiplicity due the angular de-correlations of the jets and the direction of the vector boson as explained in [15].

However background processes with $E_{\mathrm{T}}^{\mathrm{miss}}$ due to neutrinos, such as W+jets and $t\bar{t}$ tend to have more events in the positive tail. The background contribution to the high JGB (signal region) is estimated using a data driven technique based on electrons + jets + $E_{\mathrm{T}}^{\mathrm{miss}}$ selection and the estimated fake rate similarly to [10]. For electrons with $p_{\mathrm{T}} > 80\,\mathrm{GeV}$ the relevant probability for an electron to be misidentified as a photon was found to be $\sim 0.006 \pm 0.003$. The JGB distribution for events with final states with at least one electron (same as photon except for the requirement of hits on the pixel tracker matching to the supercluster), at least three jets and $E_{\mathrm{T}}^{\mathrm{miss}}$ is calculated, weighted by the misidentification rate $\mathrm{f}_{e\to\gamma}$. The difference between the population of the negative side of JGB from the corresponding on the positive side, is an additional contributor to the final background estimation.

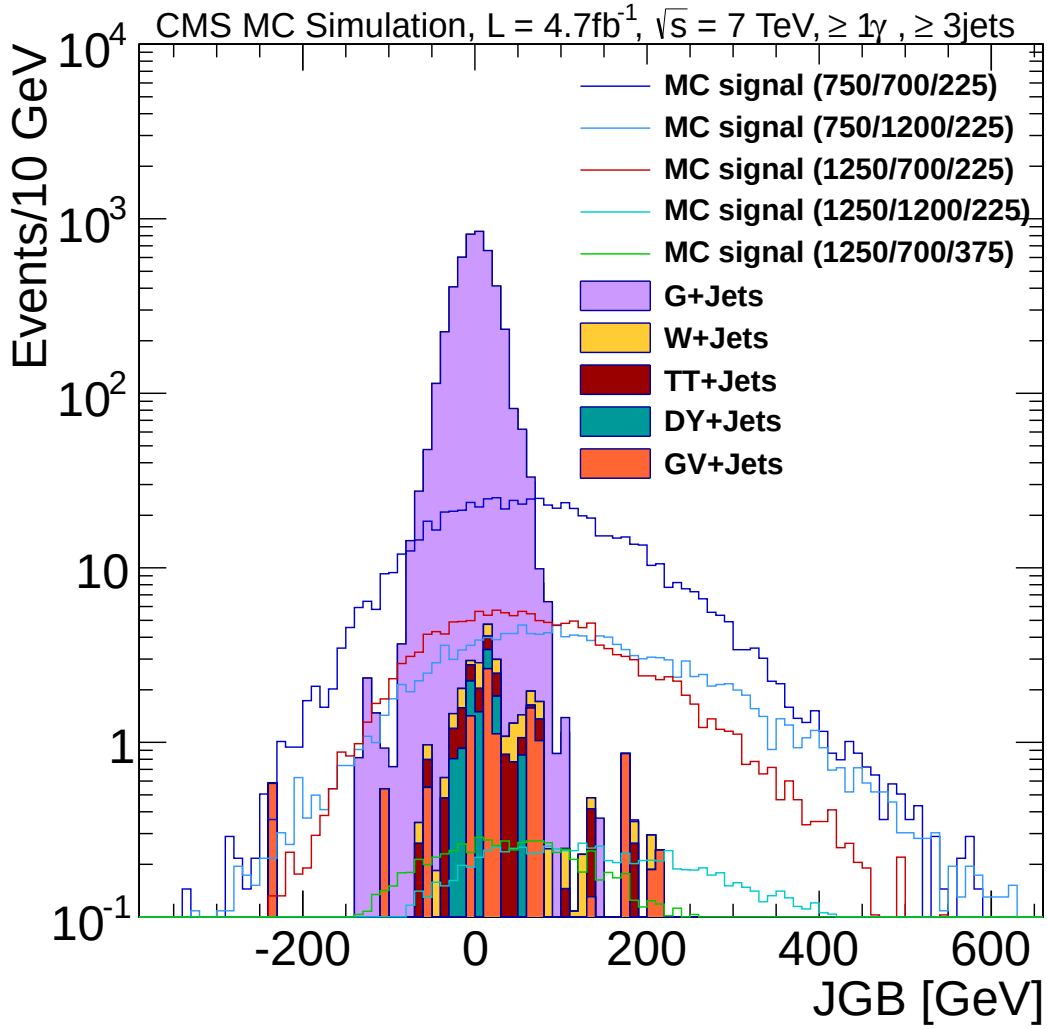

Figure 1: The JGB distribution in MC simulation for five different signals and the most important SM backgrounds ($\geq 1\gamma, \geq 3jets$).

In single jet events, the shape of the JGB distribution represents the jet energy response over the mean p_{T} spectrum of the photon production in this region of phase space. Events with an overestimated jet energy measurement will populate the JGB > 0 region, while events with an underestimated jet energy are located in JGB < 0. In multijet events the shape of the JGB distribution is the convolution of a multi jet energy measurement over the mean p_{T} spectrum of the photon production in a different region of phase space with respect to the exclusive one jet bin. Events with underestimated jets do not necessarily populate the JGB < 0 region, due to vectorial addition of the jet momenta.

To summarize, the JGB variable can be used in two ways. Firstly for the same background rejection, a JGB is more efficient than an ordinary $E_{\mathrm{T}}^{\mathrm{miss}}$ selection. Furthemore an event selection requiring positive values of JGB already rejects $\backsim$ 50% of the SM background, while retaining $\backsim$ 70% of the signal. The JGB method gives a good estimate of the total background yield expected in JGB >0, without relying on MC simulation. This is done by subtracting the JGB <0 distribution from the JGB >0 for the events with at least one electron and at least three jets, weighted by the fake rate. Then we add to this result the JGB <0 distribution for the events with at least one photon and at least three jets.

The JGB method is applied on Monte Carlo samples (Fig. 2). The predicted background distribution agrees with the observed to better than 40%, which is quoted as systematic uncertainty of the JGB background estimate. This includes both symmetric and asymmetric components.

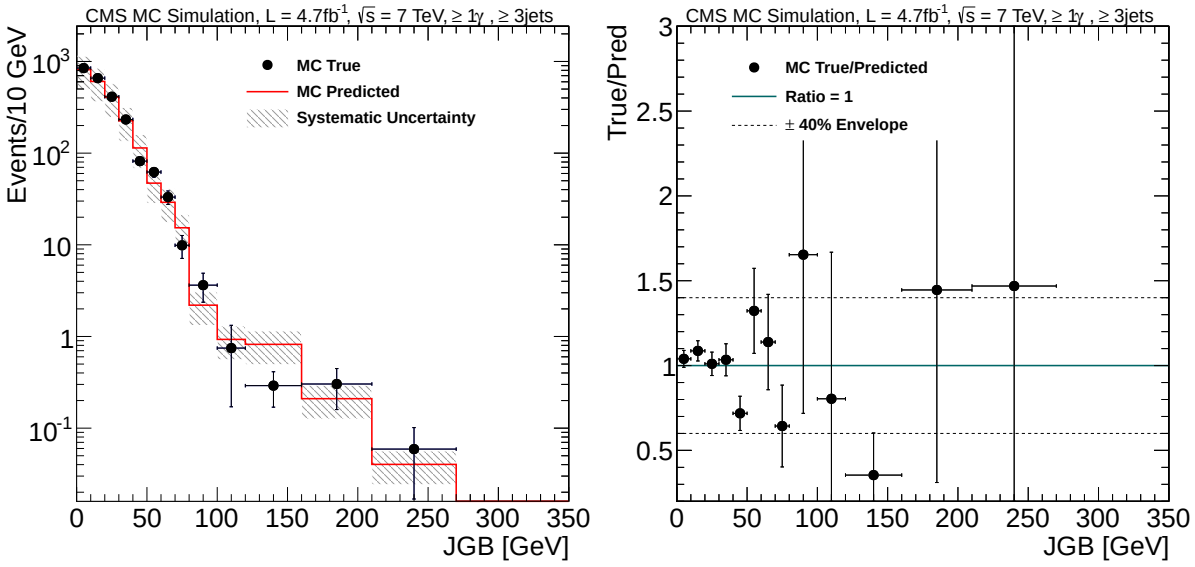

Figure 2: Monte Carlo closure test in a SM background only hypothesis ($\geq 1\gamma, \geq 3jets$). Comparison between the predicted and observed JGB distribution (left) and the ratio of the observed values versus the predicted values (right).

The Monte Carlo closure test is also repeated by mixing background with a SUSY benchmark signal (m_{squark} : 750 GeV / m_{gluino} : 700 GeV / $m_{neutralino}$: 225 GeV) to demostrate the analysis robustness under signal contamination in the control region (JGB < 0). The excess of events over the predicted background is clearly visible (Fig. 3).

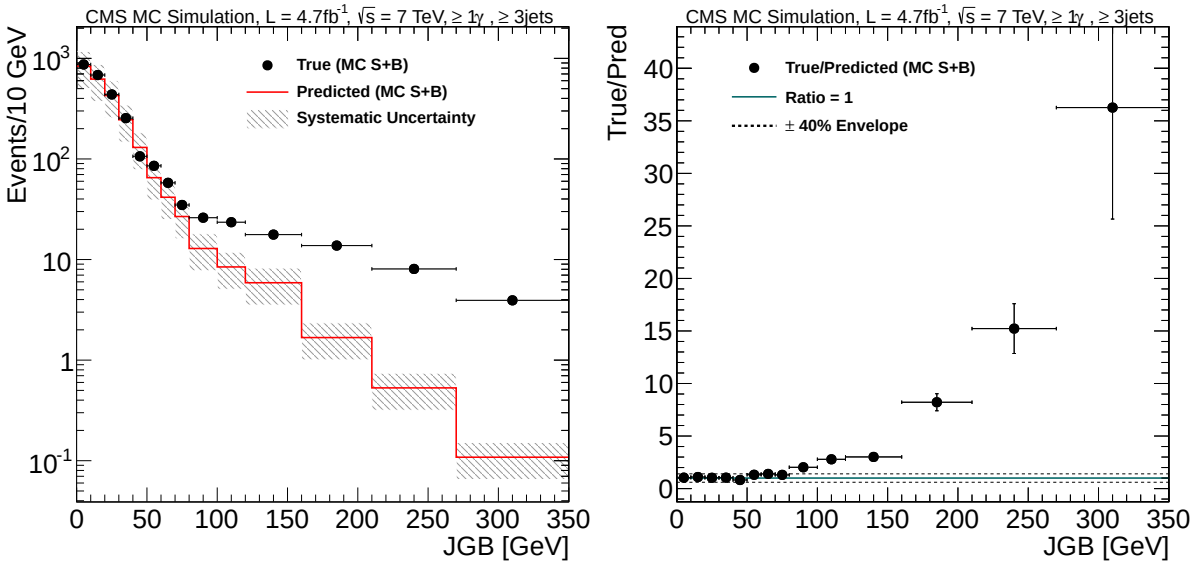

Figure 3: The JGB distribution for a MC backgrounds + signal hypothesis (left) and the ratio of the observed values vs the predicted values (right) ($\geq 1\gamma, \geq 3jets$).

6 Data Analysis

The same analysis steps are applied on data (Fig. 4). There is good agreement between observed and predicted values.

In the absence of a significant excess in the signal region over the background, exclusion limits are set on physics beyond the standard model. Three signal region bins are defined, which are used to quote the upper limits (Tab. 2). The interpretation of the analysis results is discussed in session 8.

Table 2: Total number of events observed and corresponding background prediction, in bins of JGB

$4.7\ \text{fb}^{-1}$	$80-100$ GeV			$100-120$ GeV			>120 GeV		
$\geq 1\gamma, \geq 3jets$		(stat)	(sys)		(stat)	(sys)		(stat)	(sys)
SM estimation (JGB<0)	9	$^{+4.1}_{-2.9}$	± 3.6	5	$^{+3.4}_{-2.2}$	± 2.0	3	$^{+2.9}_{-1.6}$	± 1.2
SM estimation ($f_{e\to\gamma}$)	0.3	± 0.04	± 0.1	0.3	± 0.04	± 0.1	0.9	± 0.07	± 0.4
Total SM estimation	9.3	$^{+4.1}_{-2.9}$	± 3.6	5.3	$^{+3.4}_{-2.2}$	± 2.0	3.9	$^{+2.9}_{-1.6}$	± 1.3
data	16			8			8		

7 Systematic Uncertainties

The systematic uncertainties in the signal acceptance that were taken into account for the limit calculation (experimental error band) are summarized in Table 3. The uncertainty that comes from the JGB method is 40% and is calculated using the difference between observed and predicted integrated number of events in the signal regions of the Monte Carlo closure test.

The systematic uncertainty that corresponds to Luminosity is 2.2% while the relevant uncertainty in the Jet energy scale is 2%. Possible differences in the photon identification efficiency between data and simulation are taken into account. The obtained number of events in acceptance is scaled by the ratio between the photon identification efficiency in data and simulation.

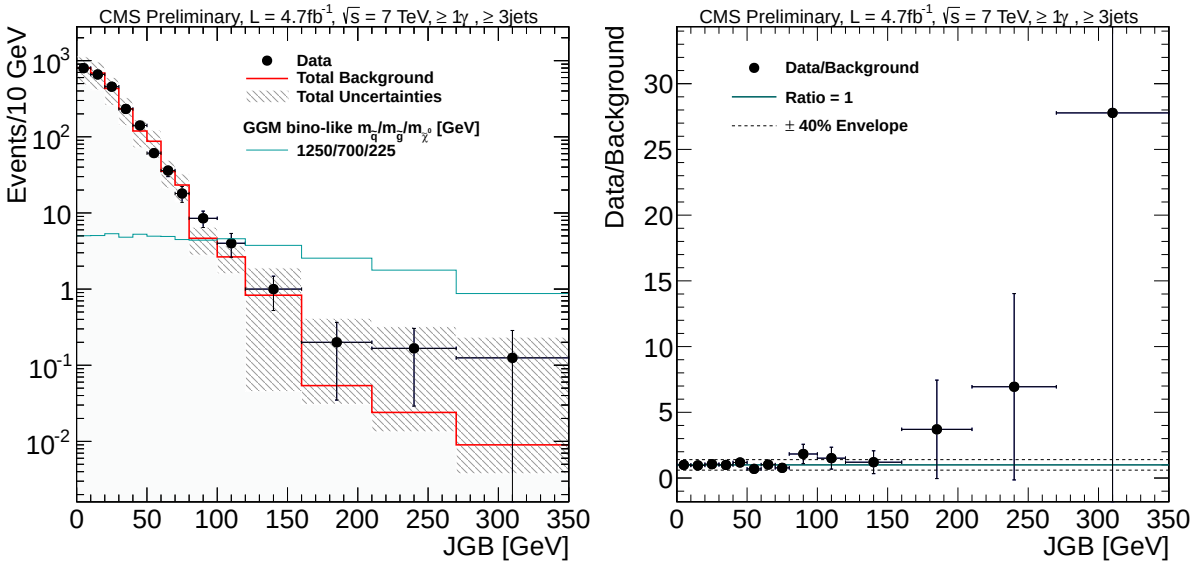

Figure 4: The JGB distribution for Data ($\geq 1\gamma, \geq 3jets$). Comparison between Observed and Predicted values (left) and the relevant ratio (right).

Table 3: List of systematic uncertainties

Source	**Uncertainty in the cross section**		
Luminosity	2.2%		
Jet energy scale	2%		
Photon efficiency	4%		
Acceptance PDF uncertainty	0.03 - 78%		
	Uncertainty in the background yield		
	80-100 GeV	100-120 GeV	$>$ 120 GeV
JGB uncertainty	39%	38%	32%
$f_{e\to\gamma}$	1%	2%	10%

These are obtained using $Z \to ee$ electrons in the data (or Monte Carlo respectively) satisfying photon identification selection (Ref. 10).

The theoretical uncertainties take into account the uncertainties in the cross section (the production cross-section at NLO is calculated using PROSPINO [16]). The relevant PDF uncertainties vary between 0.03% and 78% depending on the SUSY signal masses (increasing with larger masses of both gluino and squark).

8 Limits on physics beyond the standard model

The previous sections indicate that no clear evenidence of GGM SUSY signal was found, thus we proceed to exclusion limits' calculation using the Confidence Levels (CLs) method [17].

We calculate upper limits for GGM SUSY points for bino and wino-like neutralinos. The interpretation is done for gluino-squark mass space (both masses range from 400 to 2000 GeV with 80 GeV bin width) for a fixed neutralino mass (375 GeV). Furthemore, in the case of bino-like neutralinos, there's an interpretation for the gluino-neutralino mass plane. In this case the gluino mass ranges from 160 to 2000 GeV (80 GeV bin width), while the neutralino mass range is between 150-1050 GeV (100 GeV bin width), with a fixed squark mass (2500 GeV).

A signal point is excluded if the expected cross section exceeds our upper limit. In order to achieve good signal sensitivity, the limits were calculated for three distinct bins in GeV: [80,100), [100,120), [120,inf). Limits are set combining statistical sensitivity of the three bins.

Table 2 summarizes the observed number of events in bins of JGB as well as the corresponding background prediction with statistical and systematic uncertainties. Even though the sensitivity is dominated by the highest JGB bin, some regions of the possible signal phase-space do benefit from other bins.

The resulting 95% CL limits from these plots for a bino and wino-like neutralino scenario (with fixed neutralino mass) are summarized below.

The exclusion contours are derived from the comparison of the expected and observed cross-sections to the 95% CL upper limits. Relevant limits for a wino-like and bino-like neutralino are shown in Figure 5, Figure 6 and Figure 7. These plots also show the limits derived with the method described in SUS-12-001 [10]. The experimental error band displayed around the expected limit comes from the experimental uncertainties (see Tab. 3), while the theoretical error band comes from uncertainty in the NLO cross-section. The resulting 95% CL limits from these plots for a bino and wino-like neutralino scenario (with fixed neutralino mass) are summarized below. For the bino-like scenario with a neutralino mass fixed to 375 GeV, squark masses up to $\sim$ 900 GeV and gluino masses up to $\sim$ 920 GeV are excluded, while for the wino-like scenario with a neutralino mass fixed to 375 GeV, squark masses up to $\sim$ 870 GeV and gluino masses up to $\sim$ 770 GeV are also excluded. For the bino-like scenario with fixed squark mass (2500 GeV) and neutralino masses up to $\sim$ 350 GeV, gluino masses up to $\sim$ 950 GeV are excluded.

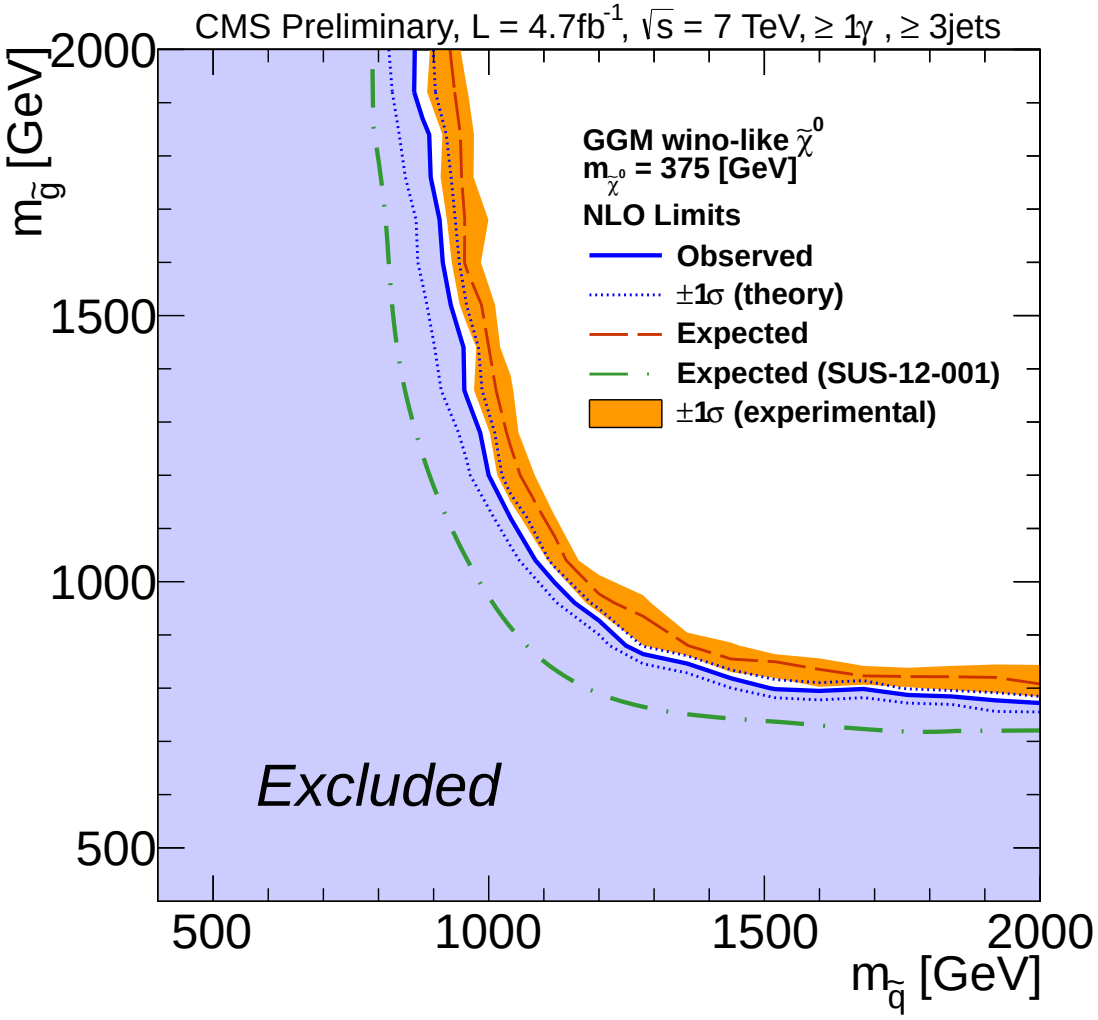

Figure 5: Calculated 95% CL exclusion contours for a wino-like neutralino in the squark-gluino mass plane.

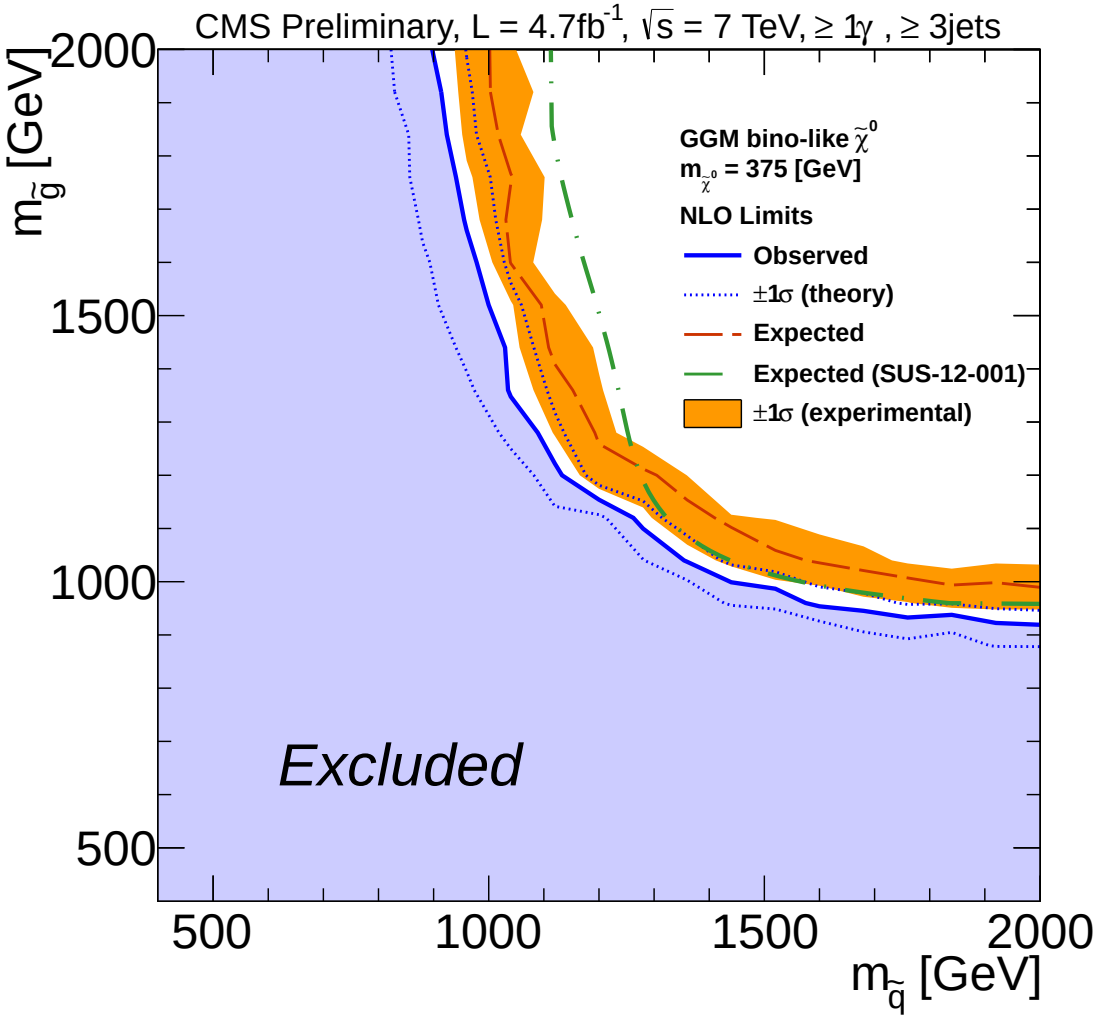

Figure 6: Calculated 95% CL exclusion contours for a bino-like neutralino in the squark-gluino mass plane.

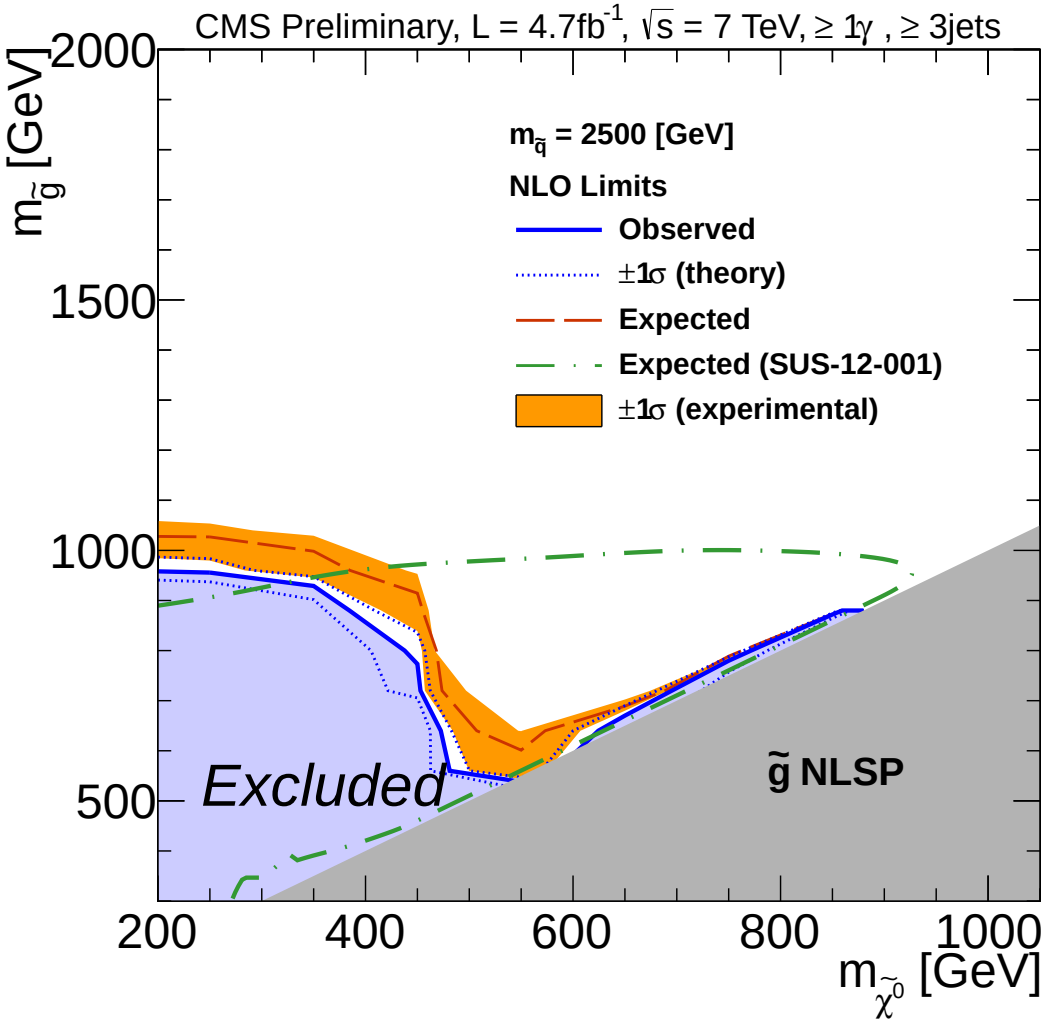

Figure 7: Calculated 95% CL exclusion contours for a bino-like neutralino in the neutralino-gluino mass plane.

9 Conclusions

In this note we have described a novel method for GGM SUSY searches in photon(s) + jets + $E_{\mathrm{T}}^{\mathrm{miss}}$ final states using 4.7 fb^{-1} of 7 TeV pp collision data collected with the CMS detector in 2011. The total background contrubution in the signal region is estimated using data control samples. Good aggrement between predicted and measured distributions are observed, both in data and MC simulation. Therefore upper limits (95% CL) are set in the GGM parameter space for several models. For the bino-like scenario with a neutralino mass fixed to 375 GeV, squark masses up to $\sim$ 900 GeV and gluino masses up to $\sim$ 920 GeV are excluded, while for the wino-like scenario with a neutralino mass fixed to 375 GeV, squark masses up to $\sim$ 870 GeV and gluino masses up to $\sim$ 770 GeV are also excluded. For the bino-like scenario with fixed squark mass (2500 GeV) and neutralino masses up to $\sim$ 350 GeV, gluino masses up to $\sim$ 950 GeV are excluded (Fig. 7).

References

[1] CMS Collaboration, "Search for Supersymmetry in Events with Photons, Jets and Missing Energy", CMS Physics Analysis Summary CMS-PAS-SUS-11-009, (2011).

[2] P. Meade et al., "General Gauge Mediation", *Prog. Theor. Phys. Suppl* **143** (2009) doi:110.1143/PTPS.177.143.

[3] M. Buican et al., "General Gauge Mediation", *European Physical Journal* **016** (2006) doi:10.1088/1126-6708/2009/03/016.

[4] A. Quadt et al., "Top quark physics at hadron colliders", *European Physical Journal* **C** (2006) doi:10.1140/epjc/s2006-02631-6.

[5] K. Theofilatos, "Supersymmetric particle detection techniques and electromagnetic calorimeter testbeam analysis with the CMS detector", phd thesis, national tech. university of athens and n.c.s.r. demokritos.

[6] CMS Collaboration, "Search for Physics Beyond the Standard Model in Z + jets + MET events at the LHC", CMS Physics Analysis Summary CMS-PAS-SUS-11-019, (2011).

[7] CMS Collaboration, "The CMS experiment at the CERN LHC", *JINST* **3** (2008).

[8] CMS Collaboration, "Photon reconstruction and identification at sqrt(s) = 7 TeV", CMS Physics Analysis Summary CMS-PAS-EGM-10-005, (2010).

[9] M. Cacciari and G. Salam, "Pileup subtraction using jet areas", *Phys. Lett.* **659** (2008) doi:10.1016/j.physletb.2007.09.077.

[10] CMS Collaboration, "Search for New Physics in Events with Photons and Missing Transverse Energy at CMS", CMS Physics Analysis Summary CMS-PAS-SUS-12-001, (2012).

[11] M. Cacciari, G. Salam, and G. Soyez, "The anti- k t jet clustering algorithm", *Journal of High Energy Physics* **04** (2008) doi:doi:10.1088/1126-6708/2008/04/063.

[12] CMS Collaboration, "Particle–Flow Event Reconstruction in CMS and Performance for Jets, Taus, and $E_{\mathrm{T}}^{\mathrm{miss}}$", *CMS Physics Analysis Summary* **CMS-PAS-PFT-09-001** (2009).

[13] CMS Collaboration, "Determination of jet energy calibration and transverse momentum resolution in CMS", *JINST* **11** (2011).

[14] A. Johan et al., "MadGraph 5: Going Beyond", *High Energy Physics - Phenomenology* (2011) doi:10.1007/JHEP06(2011)128, arXiv:1106.0522v1.

[15] CMS Collaboration, "Search for Physics Beyond the Standard Model in Z + jets + MET events at the LHC", CMS Physics Analysis Summary CMS-PAS-SUS-10-010, (2010).

[16] W. Beenakker et al., "Squark and gluino production at hadron colliders", *Nucl.Phys.* **B492** (1997) doi:10.1016/S0550-3213(97)00084-9, arXiv:hep-ph/9610490.

[17] CMS Collaboration, "Confidence Level Computation for Combining Searches with Small Statistics", *Nuclear Instruments and Methods in Physics Research* **434** (1999) doi:10.1016/S0168-9002(99)00498-2, arXiv:hep-ex/9902006v1.